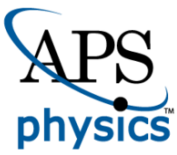

Tunable Asymmetric Transmission via Lossy Acoustic Metasurfaces

Yong Li, Chen Shen, Yangbo Xie, Junfei Li, Wenqi Wang, Steven A. Cummer, and Yun Jing

Phys. Rev. Lett. **119**, 035501 — Published 18 July 2017

DOI: 10.1103/PhysRevLett.119.035501

Tunable Asymmetric Transmission via Lossy Acoustic Metasurfaces

Yong Li,[1,2] Chen Shen,[3,4] Yangbo Xie,[3] Junfei Li,[3] Wenqi Wang,[3] Steven A. Cummer,[3,*] and Yun Jing[4,†]

[1] *Institute of Acoustics, School of Physics Science and Engineering, Tongji University, Shanghai 200092, P. R. China*

[2] *Shanghai Key Laboratory of Special Artificial Microstructure Materials and Technology, School of Physics Science and Engineering, Tongji University, Shanghai 200092, P. R. China*

[3] *Department of Electrical and Computer Engineering, Duke University, Durham, North Carolina 27708, USA*

[4] *Department of Mechanical and Aerospace Engineering, North Carolina State University, Raleigh, North Carolina 27695, USA*

(Dated: May 22, 2017)

In this study, we show that robust and tunable acoustic asymmetric transmission can be achieved through gradient-index metasurfaces by harnessing judiciously tailored losses. We theoretically prove that the asymmetric wave behavior stems from loss-induced suppression of high order diffraction. We further experimentally demonstrate this novel phenomenon. Our findings could provide new routes to broaden applications for lossy acoustic metamaterials and metasurfaces.

Ongoing development of acoustic metamaterials and metasurfaces has opened up new possibilities for controlling the behavior of sound in different acoustic media [1–6]. In most acoustic metamaterial or metasurface designs, the inherent loss is either intentionally minimized or ignored and the corresponding systems are consequently treated as Hermitian systems [7]. Indeed, losses have been conventionally considered to have an adverse effect on the performance of the acoustic material under study [8]. Losses, however, are ubiquitous in the process of acoustic wave propagation due to thermal and viscous boundary layers [9, 10] and dissipative losses [11]. Recently, there has been a growing interest in exploring new physics by embracing the losses in acoustic systems. For example, parity-time symmetric acoustic materials with carefully tailored loss and/or gain have been theoretically and experimentally demonstrated for their ability of unidirectional cloaking [12, 13], nonreciprocal reflection [14, 15], unidirectional transmission [16], topological characteristics [17] and others [18, 19].

This study, for the first time, theoretically and experimentally demonstrates asymmetric wave transmission in lossy acoustic gradient-index metasurfaces (GIM). While the theory of lossless or quasi-lossless GIMs is well studied and they have shown extraordinary ability in manipulating reflected and transmitted waves [5, 20–28], lossy GIMs are largely unexplored. This study will reveal how judiciously tailored acoustic GIMs can give rise to robust asymmetric wave transmission. In recent years, lossless passive systems or active systems also have been extensively investigated to achieve asymmetrical transmission [29–38]. However, they are in general either bulky or based on complicated designs, in which usually two functional devices (a wave vector/frequency converter and a filter) or active control is needed [29–36]. This work, in contrast, provides a new route for achieving asymmetric sound transmission by harnessing losses in metasurfaces. Finally, since the asymmetrical behavior of the proposed metasurface is highly dependent on the angle of incidence as will be shown in this paper, the "asymmetry" of the metasurface can be conveniently tuned via simple rotation.

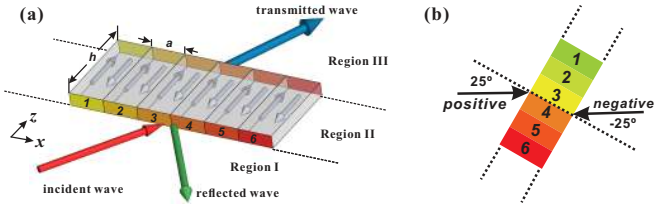

FIG. 1. (a) Schematic of wave transmitted through a gradient-index metasurface. (b) Sketch of positive and negative incidence of ±25°.

First consider a classical, lossless GIM with six unit cells per period, as depicted in Fig. 1(a), with air as the background medium. The effective refractive index of the ith unit cell is $n_i = 1 + (i-1)\,\lambda_0/mh$, where λ_0 is the wavelength at the operating frequency, $m = 6$ is the number of unit cells per period, h is the thickness of each unit cell. The transmitted phase across the unit cells $\Phi_i = \omega h n_i/c_0$ will thus cover a complete 2π range of phase shift within a period, with ω and c_0 being the angular frequency and sound speed in air, respectively.

An analytical method based on mode-coupling [26, 39, 40] is used to calculate the transmission and reflection coefficients. The entire domain is divided into three regions as illustrated in Fig. 1(a). For the pth order of diffraction mode, the x-component of wave vector along the metasurface is expressed as $G_p = k_x + 2\pi p/d$, with k_x being the wave vector of the incident wave in the x-direction and d being the length of one period. By expressing the incident, reflected and transmitted waves as summation of different modes and matching the boundary conditions, the transmission and reflection coefficients t_p and r_p for the pth order diffracted wave can be obtained [see Sup-

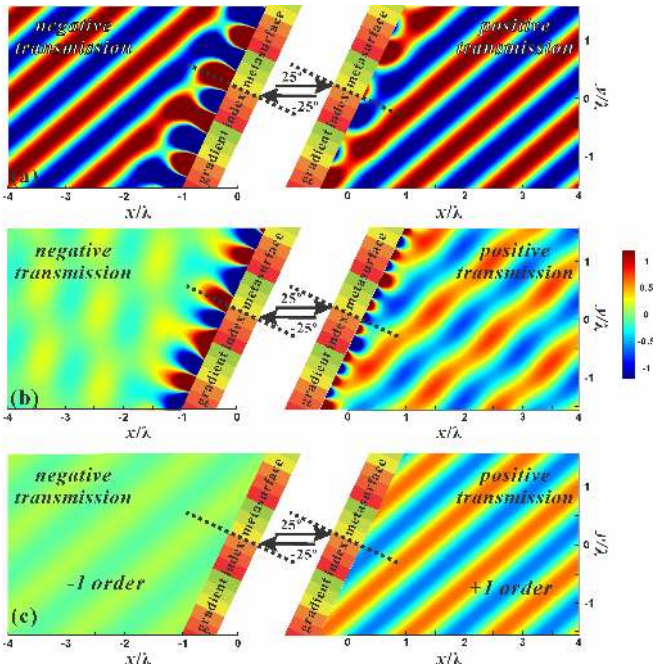

FIG. 2. Calculated acoustic pressure fields at ±25° of incidence. The left shows the transmitted field with negative incidence (−25°) and the right shows the transmitted field with positive incidence (+25°). The axes are normalized with λ. (a) Without loss in the GIM. (b) With a 0.14 loss factor in the GIM. (c) The calculated normalized transmission of ±1 propagating modes when a $\gamma = 0.14$ loss is induced.

plemental Material [41]].

We begin with the lossless case as depicted in Fig. 1(b) with positive and negative angles of incidence. The incident angle is measured from the positive (negative) z axis. Six different types of unit cells with width $a = 0.2\lambda_0$ and various refractive indices are used for the GIM. Figure 2(a) shows the acoustic pressure field immediately behind the GIM for oblique incidences at ±25°. It can be seen that the overall transmission in the far-field is almost the same for these two cases in terms of the magnitude. Now we introduce an isotropic loss in the metasurface unit cells, such that $n_i = (1 + (i-1)\,\lambda_0/mh)\,(1 + \gamma \mathrm{j})$. The corresponding acoustic pressure fields for a loss factor $\gamma = 0.14$ are displayed in Fig. 2(b). In this case, there is a stark difference between the transmission in the negative direction (−25°) and positive direction (25°): the transmission is dramatically reduced in the negative direction whereas the transmission in the positive direction is only moderately decreased.

To understand the mechanism of this peculiar asymmetric transmission, individual calculations for different diffraction orders were first performed. For the 0th order wave, the amplitude is extremely small due to the destructive interference among the unit cells [42]. We note that, at an angle of incidence of ±25°, the dominant propagating modes are of the +1 and −1 diffraction orders, respectively, as $k_{z,p} = \sqrt{k_0^2 - G_p^2}$ has to be a real value for propagating waves, or equivenlently, $k_0^2 - G_p^2 > 0$. Other modes, such as the ±2 orders, are evanescent and do not contribute to the far field transmission except at very large angles of incidence. These results, therefore, are not shown here. The corresponding acoustic pressure field for each diffraction order is presented in Fig. 2(c). The propagating mode (−1 order) is greatly suppressed for the negative direction whereas it (+1 order) is not significantly affected in the positive direction case. We further analyze why this has occurred. The generalized Snells law of gradient-index metasurfaces with phase gradient and periodic gratings reads [20, 24]:

$$(\sin\theta_t - \sin\theta_i)\, k_0 = \xi + nG \tag{1}$$

where θ_t and θ_i are angles of refraction and incidence, respectively. $\xi = \mathrm{d}\Phi/\mathrm{d}x$ is the phase gradient of the metasurface, n is the order of diffraction associated with the grating (not to be confused with the diffraction order p in Eqs. S(4)-S(7) in the Supplemental Material[41]), and $G = 2\pi/d$ is the reciprocal lattice vector. Eq. 1 implies that the overall diffraction (the one associated with p) is a result of the interplay of the phase gradient and periodic grating. Since for the current configuration of the metasurface, we have $\xi = G$, the diffraction orders can be related by $n = p - 1$. The diffraction orders associated with the gratings thus take values as $n = 0$ and $n = -2$ for the positive and negative directions, respectively (because $p = 1$ for positive direction and $p = -1$ for negative direction), which implies that the diffraction caused by the periodic gratings only takes place for the negative direction since $n = 0$ indicates that the grating term in Eq. 1 vanishes. Transient simulations of the transmitted fields through the GIM with/without loss are also performed to help reveal the underlying physics [see Supplemental Material [41]]. Remarkably, it is found that multiple reflections are enforced within the GIM for the negative direction case and are absent/negligible in the positive direction case. Since diffraction produced by the grating only takes place in the negative direction,, it is believed that the multiple reflections are associated with grating-induced high order ($p = -1$) diffractions. The multiple reflection process accumulates the energy density inside the unit cells and increases the time that wave travels therein, thus loss-induced suppression of the diffraction can be strongly enhanced and in turn gives rise to asymmetric transmission. While the above statement is true for the angle of incidence we trialed in Fig. 2, at smaller angles (those smaller than a critical angle, $\theta_c = \sin^{-1}(1 - \xi/k_0)$, which is 9.6° in this case), the 0th order diffraction ($n = 0$) dominates for both positive and negative directions[24] and therefore the multiple reflections become negligible for negative incident waves [43]. It should also be pointed out that θ_c, which is the critical angle for asymmetric transmission, can be tuned

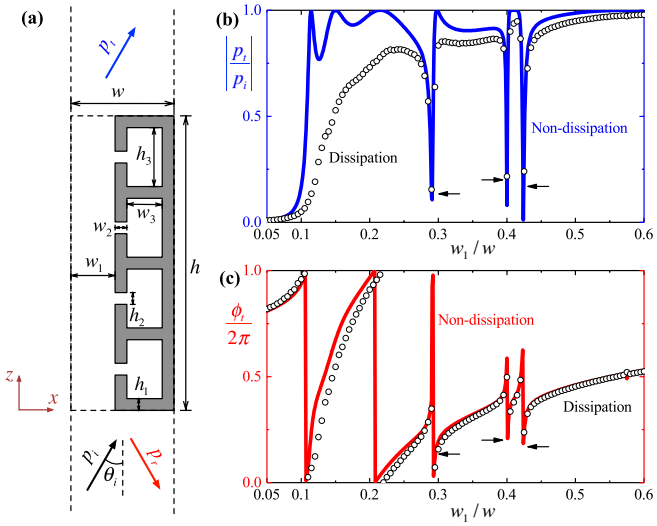

FIG. 3. (a) The schematic of the proposed metasurface unit cell consisting of four Helmholtz resonators in series connection and a straight channel. The transmission (b) amplitude and (c) phase shift of the proposed unit cell at 3430 Hz. The solid lines represent amplitude and phase shift in non-dissipative case while the open circles refer to the case with dissipation. The fluctuating peaks and dips (black arrows) stem from the resonant elastic response of the solid materials. The geometrical parameters for the simulations are $h = 4$ cm, $w = 1$ cm, $w_2 = h_1 = h_2 = 1$ mm, $h_3 = (h - 5h_1)/4$ and $w_3 = w - w_1 - w_2 - h_1$.

by the phase gradient ξ. Although the impedance matching condition of the unit cells is imposed thus far, asymmetric acoustic transmission can also be observed with impedance mismatched metasurfaces [see Supplemental Material [41]] .

To shed light on the optimal loss and angle-dependence of the asymmetric sound transmission, a series of numerical simulations have been carried out [41]. The results indicate that the optimal loss for the specific gradient index under study is around 0.12-0.15, and appreciable asymmetric transmission occurs for angles of incidence greater than 15°.

A majority of acoustic GIM designs consist of subwavelength channels and conventionally their sizes are designed to be as large as possible in order to reduce the loss and to possess high transmitted energy. However, since loss is essential here for asymmetric transmission, the GIM is intentionally designed to introduce optimal losses. Our selected unit cell, comprised of four Helmholtz resonators (HRs) in parallel connection and a straight channel on the top [27, 28], is shown in Fig. 3(a). The advantage of this type of structure is that the loss effect can be effectively tuned by the size of the HR neck, h_2, and the width of the channel, w_1. The loss from viscous friction and thermal dissipation can significantly be enhanced by reducing w_1 and h_2, since the ratio between the thickness of the viscous boundary layer and the width of the channel will increase and consequently more energy will be dissipated inside the channel and neck. The choice of the GIM structure is not restricted; other existing metasurface unit cells in principle can also be adopted here [24, 44].

The corresponding transmission spectra (amplitude, $|p_t/p_i|$, and phase shift, $\phi_t/2\pi$) of the unit cell is shown in Fig. 3(b) and they are computed using the commercial finite element package COMSOL Multiphysics [41]. The phase shift (red line) covers a 2π range when $0.15 < w_1/w < 0.6$. Compared with the amplitude profile (blue line) in the non-dissipative case, the transmitted amplitude (open circles) drops with the decrease of w_1, providing solid proof of the existence of dissipation. The Fano-like resonance (black arrow) exhibited in Fig. 3 is the coupling resonance between the solid resonant states of the thin walls and Helmholtz resonance.

According to the phase profile [cf. Fig. 3(b)], 6 units are selected with a step-size of $\pi/3$ to construct the GIM. The average effective loss factor of these unit cells is estimated to be around 0.14 [41]. The phase gradient is selected as $\xi = \pi/6h$ (each unit repeats once within a period, so that 12 units form a period) and subsequently the GIM can be established based on the desired phase profile. The spatial resolution of each element is $w = a/2 = \lambda_0/10$, which is sufficiently fine to ensure accurate phase modulation. Full wave simulations with and without losses were performed to validate the proposed GIM. The asymmetric pressure fields of the GIM under the positive and negative incidence directions can be found in the Supplemental Material [41].

Measurements of the 3D printed GIM were conducted in a 2D waveguide. The experimental setup is shown in Fig. 4 and θ is the rotation angle of the GIM relative to the original position (normal to the wavefront). The acoustic field is scanned using a moving microphone with a step size of 2 cm behind the GIM. The measured acoustic fields are depicted in Fig. 4 at the angle of incidence of $\pm 25°$. Good agreement is found between the simulations [See Fig. S5 in the Supplemental Material [41]] and the measurements, which are both consistent with the theory. For the negative direction case, most of the acoustic energy is concentrated on the surface of the GIM, confirming the strong attenuation of the propagating wave through the GIM.

To quantify the performance of the prototype, we further examine the transmitted energy contrast (the ratio between the transmitted energy from the positive direction and the negative direction) by integrating the acoustic intensity along a line parallel to the GIM with distance two wavelengths away. The corresponding results are presented in Fig. 5. The experimental result shows good agreement with the simulation result. The peak contrast is greater than 10 times (10 dB) at an incident angle of 25°. The strongly asymmetric incidence angles, defined by their contrast being greater than 6, range approxi-

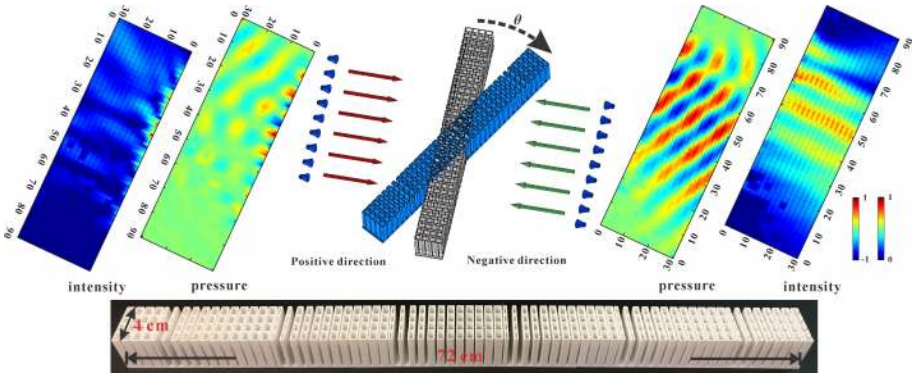

FIG. 4. Measured transmitted acoustic fields at $\theta = 25°$. The left and right panels show the measured acoustic fields of negative direction ($-25°$) and positive direction ($+25°$), respectively. The middle panel shows the experiment setup. The left (right) incidence corresponds to the positive (negative) direction case. A photo of the fabricated prototype is shown in the bottom panel. Axes unit: cm.

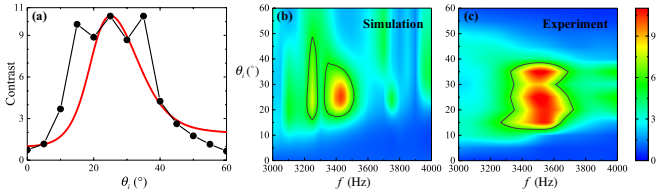

FIG. 5. (a) Energy contrast with different angles of incidence at 3430 Hz (red curve: simulation; black circles: measurement). (b) Simulated and (c) experimentally obtained energy contrast as a function of frequency, f, and the angle of incidence, θ_i. The black curves represent the region in which contrast is greater than 6 (7.8 dB).

mately from 15° to 40° as observed from experiments. At small angles of incidence (e.g., $0-5°$), the energy contrast is close to unity and the sound transmission is symmetrical. Consequently, tunable sound transmission contrast ratio (transmission asymmetry) can be realized by mechanically or electronically rotating the GIM in order to adjust the angle of incidence. To investigate the frequency-dependence of the asymmetrical transmission behavior, 2D maps of the energy contrast (energy contrast vs. angle of incidence vs. frequency) are generated from both the simulation and experiment, where reasonable agreements are observed. The area of high energy contrast is confined to a region with frequencies ranging approximately from $3.4-3.6$ kHz and angles ranging from $15-40°$. The contrast ratio is around 1 at small angles of incidence and gradually increases with the incident angle. At large angles of incidence ($> 45°$), the contrast ratio drops because the transmission for the positive direction decreases due to impedance mismatch [45].

To conclude, we have theoretically and experimentally demonstrated asymmetric transmission through lossy GIMs with tailored internal losses. We show that the asymmetric wave behavior is due to loss-induced suppression of high order diffractions. In both theoretical prediction and measurements, asymmetric transmission can be clearly observed within a range of incident angles and frequencies. The asymmetrical behavior is also tunable by adjusting the orientation of the metasurface since it is highly dependent on the angles of incidence. The usefulness of losses in acoustic metamaterials/metasurfaces for sound transmission manipulation is largely unexplored, and it is shown here that, losses can be harnessed to create robust asymmetric transmission. It is hoped that this study could open up new possibilities in the family of lossy acoustic metamaterials and metasurfaces as it adds another degree of freedom to the control of sound transmission. The theory presented here can be possibly extended to benefit other areas of lossy physical systems, such as electromagnetic waves.

This work was supported by a Multidisciplinary University Research Initiative grant from the Office of Naval Research (N00014-13-1-0631) and an Emerging Frontiers in Research and Innovation grant from the National Science Foundation (Grant No. 1641084). Y.L. acknowledges a stat-up fund from Tongji University.

Y.L. and C.S. contributed equally to this work.

* cummer@duke.edu
† yjing2@ncsu.edu

[1] Z. Liu, X. Zhang, Y. Mao, Y. Y. Zhu, Z. Yang, C. T. Chan, and P. Sheng, Science **289**, 1734 (2000).
[2] N. Fang, D. Xi, J. Xu, M. Ambati, W. Srituravanich, C. Sun, and X. Zhang, Nat. Mater. **5**, 452 (2006).
[3] Z. Yang, J. Mei, M. Yang, N. H. Chan, and P. Sheng, Phys. Rev. Lett. **101**, 204301 (2008).
[4] S. A. Cummer, J. Christensen, and A. Alu, Nat. Rev. Mat. **1**, 16001 (2016).
[5] G. Ma and P. Sheng, Sci. Adv. **2**, e1501595 (2016).
[6] T. Y. Huang, C. Shen, and Y. Jing, J. Acoust. Soc. Am. **139**, 3240 (2016).
[7] C. M. Bender, Rep. Prog. Phys. **70**, 947 (2007).

[8] G. P. Ward, R. K. Lovelock, A. R. Murray, A. P. Hibbins, J. R. Sambles, and J. D. Smith, Phys. Rev. Lett. **115**, 044302 (2015).

[9] Y. Li and B. M. Assouar, Appl. Phys. Lett. **108**, 063502 (2016).

[10] M. Molerón, M. Serra-Garcia, and C. Daraio, New J. Phys. **18**, 033003 (2016).

[11] P. M. Morse and K. U. Ingard, *Theoretical Acoustics* (Princeton University Press, Princeton, 1987).

[12] R. Fleury, D. Sounas, and A. Alu, Nat. Commun. **6**, 5905 (2015).

[13] X. F. Zhu, H. Ramezani, C. Z. Shi, J. Zhu, and X. Zhang, Phys. Rev. X **4**, 031042 (2014).

[14] J. Christensen, EPL **114**, 47007 (2016).

[15] J. Christensen, M. Willatzen, V. R. Velasco, and M. H. Lu, Phys. Rev. Lett. **116**, 207601 (2016).

[16] Z. M. Gu, J. Hu, B. Liang, X. Y. Zou, and J. C. Cheng, Sci. Rep. **6**, 19824 (2016).

[17] K. Ding, G. C. Ma, M. Xiao, Z. Q. Zhang, and C. T. Chan, Phys. Rev. X **6**, 021007 (2016).

[18] R. Fleury, D. L. Sounas, and A. Alu, IEEE J. Sel. Topics Quantum Electron. **22**, 121 (2016).

[19] L. Xiong, W. Bi, and Y. Auregan, J. Acoust. Soc. Am. **139**, 764 (2016).

[20] N. Yu, P. Genevet, M. A. Kats, F. Aieta, J. P. Tetienne, F. Capasso, and Z. Gaburro, Science **334**, 333 (2011).

[21] N. Yu and F. Capasso, Nat. Mater. **13**, 139 (2014).

[22] Y. Li, B. Liang, Z. M. Gu, X. Y. Zou, and J. C. Cheng, Sci. Rep. **3**, 2546 (2013).

[23] Y. Li, X. Jiang, R. Q. Li, B. Liang, X. Y. Zou, L. L. Yin, and J. C. Cheng, Phys. Rev. Applied **2**, 064002 (2014).

[24] Y. Xie, W. Wang, H. Chen, A. Konneker, B. I. Popa, and S. A. Cummer, Nat. Commun. **5**, 5553 (2014).

[25] K. Tang, C. Qiu, M. Ke, J. Lu, Y. Ye, and Z. Liu, Sci. Rep. **4**, 6517 (2014).

[26] J. Mei and Y. Wu, New J. Phys. **16**, 123007 (2014).

[27] Y. Li, X. Jiang, B. Liang, J. C. Cheng, and L. K. Zhang, Phys. Rev. Applied **4**, 024003 (2015).

[28] X. Jiang, Y. Li, B. Liang, J. C. Cheng, and L. Zhang, Phys. Rev. Lett. **117**, 034301 (2016).

[29] B. Liang, B. Yuan, and J. C. Cheng, Phys. Rev. Lett. **103**, 104301 (2009).

[30] B. Liang, X. S. Guo, J. Tu, D. Zhang, and J. C. Cheng, Nat. Mater. **9**, 989 (2010).

[31] N. Boechler, G. Theocharis, and C. Daraio, Nat. Mater. **10**, 665 (2011).

[32] X. F. Zhu, X. Y. Zou, B. Liang, and J. C. Cheng, J. Appl. Phys. **108**, 124909 (2010).

[33] X. F. Li, X. Ni, L. Feng, M. H. Lu, C. He, and Y. F. Chen, Phys. Rev. Lett. **106**, 084301 (2011).

[34] R. Fleury, D. L. Sounas, C. F. Sieck, M. R. Haberman, and A. Alu, Science **343**.

[35] B. I. Popa and S. A. Cummer, Nat. Commun. **5**, 3398 (2014).

[36] T. Devaux, V. Tournat, O. Richoux, and V. Pagneux, Phys. Rev. Lett. **115**, 234301 (2015).

[37] C. Shen, Y. B. Xie, J. F. Li, S. A. Cummer, and Y. Jing, Appl. Phys. Lett. **108**, 223502 (2016).

[38] B. Xie, H. Cheng, K. Tang, Z. Liu, S. Chen, and J. Tian, Phys. Rev. Applied **7**, 024010 (2017).

[39] F. Y. Cai, F. M. Liu, Z. J. He, and Z. Y. Liu, Appl. Phys. Lett. **91**, 203515 (2007).

[40] J. Christensen, L. Martin-Moreno, and F. J. Garcia-Vidal, Phys. Rev. Lett. **101**, 014301 (2008).

[41] See Supplemental Material at url for more detailed discussions on analytical derivations, physical mechanism and loss contribution.

[42] E. T. Qian, Y. Y. Fu, Y. D. Xu, and H. Y. Chen, EPL **114**, 34003 (2016).

[43] W. Wang, Y. Xie, B.-I. Popa, and S. A. Cummer, J. Appl. Phys. **120**, 195103 (2016).

[44] X. Zhu, K. Li, P. Zhang, J. Zhu, J. Zhang, C. Tian, and S. Liu, Nat. Commun. **7**, 11731 (2016).

[45] Y. Li, S. Qi, and M. B. Assouar, New J. Phys. **18**, 043024 (2016).